Theoretical and Applied Fracture Mechanics 131 (2024) 104424

Contents lists available at ScienceDirect

Theoretical and Applied Fracture Mechanics

journal homepage: www.elsevier.com/locate/tafmec

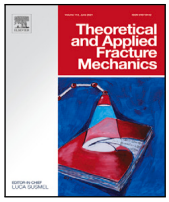

Multiscale modelling of composite laminates with voids through the direct FE^2 method

Bruno G. Christoff [a], José Humberto S. Almeida Jr. [b,c,*], Marcelo L. Ribeiro [d], Maísa M. Maciel [d], Rui M. Guedes [a,e], Volnei Tita [a,d]

[a] Department of Mechanical Engineering, Faculty of Engineering of the University of Porto, Porto, Portugal
[b] School of Mechanical and Aerospace Engineering, Queen's University Belfast, Belfast, UK
[c] Department of Mechanical Engineering, LUT University, Lappeenranta, Finland
[d] Department of Aeronautical Engineering, São Carlos School of Engineering, University of São Paulo, São Carlos, SP, Brazil
[e] LAETA, UMAI-INEGI, Portugal

ARTICLE INFO

Keywords:
FE^2 method
Multiscale modelling
Voids
Global-local approach

ABSTRACT

A concurrent multiscale method, namely the direct FE^2, is developed to analyse the mechanical response of fibre-reinforced composites with several void fractions in a nested manner, one at the macro and another one at the microscale. The FE^2 is developed through the finite element (FE) mesh at the macro scale, wherein there is a representative volume element (RVE) at every Gauss point where the strains and stresses are evaluated. The RVEs, located at macroscopic FE mesh, with linear boundary conditions applied to the boundary nodes, are linked to macro-scale nodes via Multi-Point Constraints (MPCs). This procedure enables solving a single equilibrium problem, with boundary conditions and loadings at the macro scale and provides data for all defined RVEs. The methodology is applied to a composite laminate under transverse tension. Initially, the method is evaluated to compare the results from the FE^2 with those from analyses where the entire domain is discretised (conventional FE full-scale modelling). The stresses obtained from the FE^2 method match traditional FE analyses but utilise a significantly lower number of finite elements, resulting in substantial computational cost savings. It follows a parametric study of void distribution effects within the RVE. Afterwards, the stress distribution within the RVE is assessed and then failure of the composites is predicted at the macro scale through the stresses and strains concurrently calculated at the micro-scale.

1. Introduction

The mechanical performance of heterogeneous structures is often challenging to model since considering microscopic features in the macroscopic model through homogenisation techniques e.g., asymptotic homogenisation method [1], and several analytical and semi-analytical methods [2] is computationally exhaustive. Multiscale methods are usually a class of approaches used to overcome this issue, where the mechanical response of the system at the macroscale can be derived from the microscale, which is often formulated using a representative unit cell (RUC) or a representative volume element (RVE) [3,4]. These can provide sufficient information about the level of heterogeneity in the media once they consider the various constituents of the solid and their associated mechanical behaviour [5]. Then, mechanical behaviour can be exported or used concomitantly with the model on a larger scale, for example, on the meso scale, where the different phases of the solid are homogenised [6].

Multiscale methods to model fibre-reinforced composites can be subdivided into two categories: sequential (hierarchical) and concurrent methods. In a nutshell, in sequential approaches [7], information about the interaction between the phases (e.g., fibre, matrix) is lost when moving from the constituent (micro) to the homogenised (macro) level [8]. The main issue is when the interaction between phases needs to be carefully considered, given that it can greatly influence the damage processes of the composite system [9], especially when strain localisation is established. Concurrent methods, nonetheless, continuously store information regarding both micro and macro levels in the same "global" model since they exchange information with each other at every step of the global analysis. The key advantage of concurrent methods is the 'live' consideration of the interaction between the different phases of the media since every step of the analysis contains current information from both scales [8,10].

* Corresponding author.
E-mail addresses: humberto.almeida@qub.ac.uk, humberto.almeida@lut.fi (J.H.S. Almeida Jr.).

https://doi.org/10.1016/j.tafmec.2024.104424
Received 2 October 2023; Received in revised form 13 March 2024; Accepted 10 April 2024
Available online 19 April 2024

A suitable concurrent multiscale method to simulate the mechanical behaviour of fibre-reinforced composites is the FE^2, which consists of two nested continuum models requiring constitutive assumptions only at the local level (RVE) [11,12]. The FE^2 method requires the simultaneous computation of the mechanical response of the media on two scales, that is, the homogenised structure on the macroscale receives information from the underlying heterogeneous system on the microscale employing an RVE, where strains and stresses are computed at every Gauss point [10].

The FE^2 method is not widely applied to simulate the mechanical behaviour of composites, as can be seen in the review by Raju et al. [13]. For example, Feyel [14] used the FE^2 to simulate the elastoviscoplastic behaviour of SiC/Ti composites. Nezamabadi et al. [11] modelled the compressive failure of composites using the FE^2 method. Nezamabadi et al. [15] also used the FE^2 method to simulate the instability phenomena in composite materials, allowing buckling to occur at both macroscopic and microscopic length scales. Tan et al. [16] showed how the separate FE models from the two scales that are typical of FE^2 analyses can be merged into one global approach. Tikarrouchine et al. [17] proposed a FE^2 methodology to predict the non-linear macroscopic response of composite structures with a time-dependent response. Herwig and Wagner [18] applied the FE^2 method to model delamination in composites. Zhi et al. [19] solved dynamic problems in composites through the Direct FE^2 method. Later, Zhi et al. [20] extended their framework toward a micromorphic continuum capable of capturing the deformation of composites with soft inclusions. They [21] also used the same approach to solve the thermo-viscoelastic behaviour of the curing kinetics of laminated composites. Koyanagi et al. [22] used the same method to simulate the strain-rate dependence of composite cylinders in compression. Raju et al. [23] analysed the nonlinear shear and damage behaviour of angle-ply composite laminates using a Direct FE^2 approach. This state-of-the-art reveals that the FE^2 method is effective in the modelling of composite structures. However, none of these studies considers defects in the composite system in their models.

In this context, this paper aims to bridge the macro and micro scales in fibre-reinforced composites through the Direct FE^2 as an alternative to both mono-scale and sequential multiscale models. For the first time, both the type and the content of voids are assessed at the micro level through RVEs, in which their kinematics (stresses and strains) are locally evaluated at every Gauss point (GP) of the macro FE mesh, and are concurrently exchanged with the homogenised model at the macro scale, where the loads (transverse tension) and boundary conditions (BCs) are applied. The RVEs are located at every GP of the macro finite element (FE) mesh, thus characterising the FE^2 global model.

2. The formulation

2.1. The approach

The concept of RVE is used to describe the heterogeneous media. A periodic elastic body is considered, and the problem is formulated in the bounded subset $\Omega \in R^2$. Two scales are used to represent the media, one at the micro level (RVE) and one at the macro level. The nomenclature adopted follows [1,4,24]. The micro and macro domains are defined by

$$\boldsymbol{Y} = \{\boldsymbol{y} = (y_1, y_2) \in \mathbb{R}^2 : 0 < y_i < l_i, i = 1,2\}, \tag{1}$$

and

$$\Omega = \{\boldsymbol{x} = (x_1, x_2) \in \mathbb{R}^2 : 0 < x_i < L_i, i = 1,2\}, \tag{2}$$

where $\boldsymbol{y}$ and $\boldsymbol{x}$ represent the coordinates at the microscale and macroscale, respectively ($\boldsymbol{l}$ and $\boldsymbol{L}$ are positive numbers). Both the microscale and macroscale domains are discretised by finite elements, such that

$$Y = \biguplus_{e=1}^{n_e} Y^{(e)}, \tag{3}$$

and

$$\Omega = \biguplus_{e=1}^{N_e} \Omega^{(e)}, \tag{4}$$

where n_e and N_e are the number of elements used to discretise the RVE and the macroscopic domain, respectively.

Ideally, in multiscale problems, there is a clear separation between the scales defined for the domains, such that

$$\boldsymbol{y} = \frac{\boldsymbol{x}}{\varepsilon}, \tag{5}$$

where $\varepsilon \ll 1$ means that the microscopic domain is significantly smaller than the macroscopic one. However, achieving a distinct separation between these scales is not always feasible. Here, the microscale is regarded as a single point within the macroscale domain. The effective average properties, determined through analyses on RVEs, are applied to the Gauss points of the FE mesh within the macroscale domain. This becomes true in a limit analysis [25]. For cases where this limit does not apply, we can consider multiscale methods as approximations.

In the approach herein considered, loads and boundary conditions are directly applied to the macroscopic domain. Fig. 1 presents a schematic representation of the virtual tensile test under consideration.

For the macroscopic domain Ω, the Dirichlet and Neumann boundary conditions are applied [26] on the boundaries $\partial\Omega_u$ and $\partial\Omega_f$, respectively, where

$$\Gamma = \partial\Omega_{u_i} \cup \partial\Omega_{f_i}; \quad \partial\Omega_{u_i} \cap \partial\Omega_{f_i} = \varnothing \quad i = 1,2. \tag{6}$$

For the microscopic domain Y, we employ an idealised model in which the medium is represented by an RVE consisting of a centrally positioned fibre surrounded by the matrix. In the analyses, we also consider defects within the RVE, which will be represented by voids within the matrix.

The direct FE^2 model is constructed with the assumption that the RVEs are positioned at all Gauss points of the macroscopic FE mesh, under prescribed BCs and considering the energy balance between external and internal work within the medium. The macroscopic FE mesh serves as a reference for placing the RVEs and applying BCs. The resulting equilibrium outcomes will show the fields of interest across all the RVEs defined within the direct FE^2 model. Therefore, this approach involves performing a multiscale concurrent analysis in a single step, where both the macroscopic and microscopic domains are integrated into a unified analysis.

2.2. The direct FE^2 formulation

Let $\delta\boldsymbol{u}$ be a kinematically admissible virtual displacement. The principle of virtual work asserts that an elastic body is in equilibrium if and only if the external virtual work equals the internal virtual work, as

$$W_{ext} = W_{int}. \tag{7}$$

The external virtual work is defined as

$$W_{ext} = \int_{\Omega} b_i \delta u_i d\Omega + \int_{\Gamma} t_i \delta u_i d\Gamma, \tag{8}$$

where $\boldsymbol{\sigma}$ is the stress tensor, $\boldsymbol{b}$ are the body forces, and $\boldsymbol{t}$ is the traction vector. The internal virtual work is defined as

$$W_{int} = \int_{\Omega} \sigma_{ij} \delta u_{i,j} d\Omega. \tag{9}$$

Considering a quadrature scheme for evaluating the integrals, one can write the expression for the internal virtual work, Eq. (9), as

$$W_{int} = \sum_{e=1}^{Ne} \sum_{m=1}^{P} \left(\sigma_{ij}^{(e)(m)} \delta u_{i,j}^{(e)(m)} \right) W_m J_m, \tag{10}$$

where P is the number of quadrature points used in the integration; W_m and J_m are, respectively, the quadrature weight and the determinant

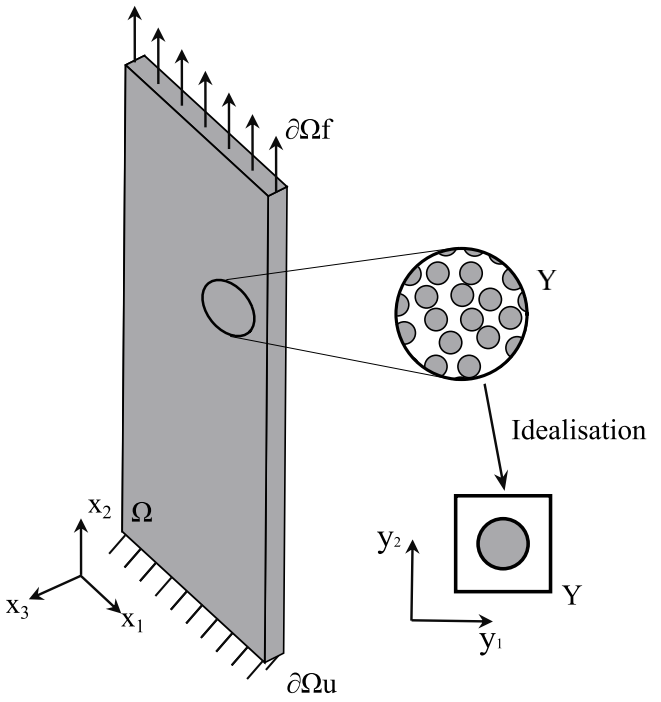

Fig. 1. Virtual transverse tensile test on a fibre-reinforced laminate, with the adopted definition of both macroscopic and microscopic domains under consideration.

of the Jacobian matrix, which are associated with the mth quadrature point.

In multiscale problems, it is considered that the stresses at individual Gauss points within the macroscopic domain are obtained as the averages of the stresses calculated within the corresponding RVEs. Consequently, we assume that Eq. (10) can be formulated as

$$W_{int} = \sum_{e=1}^{Ne} \sum_{m=1}^{P} \langle \tilde{\sigma}_{ij} \rangle^{(e)(m)} \langle \delta \tilde{u}_{i,j} \rangle^{(e)(m)} W_m J_m, \tag{11}$$

where $\tilde{\bullet}$ represents a field dependent on the microscopic scale, and the average operator $\langle \bullet \rangle$ is defined as

$$\langle \bullet \rangle = \frac{1}{|Y|} \int_Y \bullet \, dY, \tag{12}$$

where $|Y|$ is the volume of the RVE.

Considering the Hill–Mandel condition for homogenisation given by

$$\langle \tilde{\sigma}_{ij} \rangle \langle \delta \tilde{u}_{i,j} \rangle = \langle \delta \tilde{\sigma}_{ij} \tilde{u}_{i,j} \rangle \tag{13}$$

one can write Eq. (11), considering Eq. (12), as

$$W_{int} = \sum_{e=1}^{Ne} \sum_{m=1}^{P} \frac{W_m J_m}{|Y|} \int_Y \tilde{\sigma}_{ij}^{(e)(m)} \delta \tilde{u}_{i,j}^{(e)(m)} dY, \tag{14}$$

which is an expression for the virtual internal work within the macroscopic domain, expressed concerning the fields within the microscopic domain.

It is worth noting that if we directly sum the internal work of all the RVEs, we get

$$\tilde{W}_{int} = \sum_{e=1}^{Ne} \sum_{m=1}^{P} \left(\int_Y \tilde{\sigma}_{ij}^{(e)(m)} \delta \tilde{u}_{i,j}^{(e)(m)} dY \right). \tag{15}$$

By comparing Eqs. (14) and (15), we can see that the virtual internal work in the macroscopic domain and the virtual internal work in the microscopic domain differ by a scale factor equal to

$$\tilde{W} = \frac{W_m J_m}{|Y|} \tag{16}$$

which can be seen as a scaling factor to the problem. On a closer examination of Eq. (16), one can observe that it represents a connection between the volume of the macroscale (associated with the Gauss Point of a specific element of the FE mesh) and the volume of the corresponding RVE. For 2D problems, this relation is satisfied by multiplying the thickness of the RVE by the factor $\tilde{W}$. Therefore, the energy balance given in Eq. (7) with the external work Eq. (8) and the internal work Eq. (14), can be written as

$$\int_\Omega b_i \delta u_i d\Omega + \int_\Gamma t_i \delta u_i d\Gamma = \sum_{e=1}^{Ne} \sum_{m=1}^{P} \frac{W_m J_m}{|Y|} \int_Y \tilde{\sigma}_{ij}^{(e)(m)} \delta \tilde{u}_{i,j}^{(e)(m)} dY. \tag{17}$$

Noteworthy, the left-hand side (LHS) of Eq. (17) depends exclusively on the macroscale domain, while the right-hand side (RHS) depends only on the microscale domain. This equation deduced from the theory provides a clear connection between the external work in the macroscopic mesh and the internal work within the RVEs.

The Eq. (17) can be reformulated in the standard finite element form. After some algebraic manipulations, and considering no body forces, it can be expressed as

$$\tilde{K}_{ij} \tilde{d}_j \delta \tilde{d}_i = f_k \delta d_k, \tag{18}$$

where $\tilde{\boldsymbol{d}}$ represents the nodal displacement field within the RVEs, $\delta \tilde{\boldsymbol{d}}$ and $\delta \boldsymbol{d}$ are the virtual displacement fields at the microscopic and macroscopic scales, respectively. Moreover, $\tilde{\boldsymbol{K}}$ is the stiffness matrix, which is constructed by assembling the contributions from all the RVEs within the FE^2 model.

In Eq. (18), both macroscopic and microscopic fields are depicted. In first-order homogenisation problems, it is possible to establish a linear relationship between the nodal macroscopic and microscopic displacement fields, as

$$d_k = L_{ik} \tilde{d}_i, \tag{19}$$

where $\boldsymbol{L}$ is a linear operator that establishes a linear relationship between the displacement field at the boundaries of the RVE and the nodal displacement field of the macroscopic element.

Taking into account Eq. (19) and recognising that virtual displacements can be arbitrary, we can rewrite the equilibrium problem of Eq. (18) as

$$\tilde{K}_{ij} \tilde{d}_i = L_{ik} f_k. \tag{20}$$

The Eq. (20) demonstrates how both scales are merged into a single simulation using the direct FE^2 method. The stiffness matrix of the RVEs is scaled by a factor $\tilde{W}$ (as per Eq. (16)), and the nodal forces of the problem are mapped between the micro and macro fields through the matrix $\boldsymbol{L}$, Eq. (19). The explicit derivation of the matrix $\boldsymbol{L}$ is unnecessary because most finite element software, such as Abaqus, supports linear Multiple-point constraints (MPCs), which enable linear constraints between nodes. In this context, the displacement fields on the boundary of every RVE are interpolated with the macroscale displacement fields using macroscale shape functions. This BC applied to the RVE is referred to as the Voigt-Taylor model.

2.3. The procedure

Fig. 2 shows a flowchart of the developed procedure to solve the equilibrium problem. The FE software Abaqus® is utilised for pre-processing, post-processing, and solving the equilibrium problem, while Python language is employed to position the RVEs and automate the application of BCs at the microscale.

The procedure starts with the definition of the macroscale model, discretising the geometry and generation of the FE mesh for the macroscale model by using quadrilateral (S4 in Abaqus reference) finite elements. After the element type is defined, it then determines the number of Gauss points within a single macroscopic element and, consequently, the number of RVEs within the direct FE^2 model. When

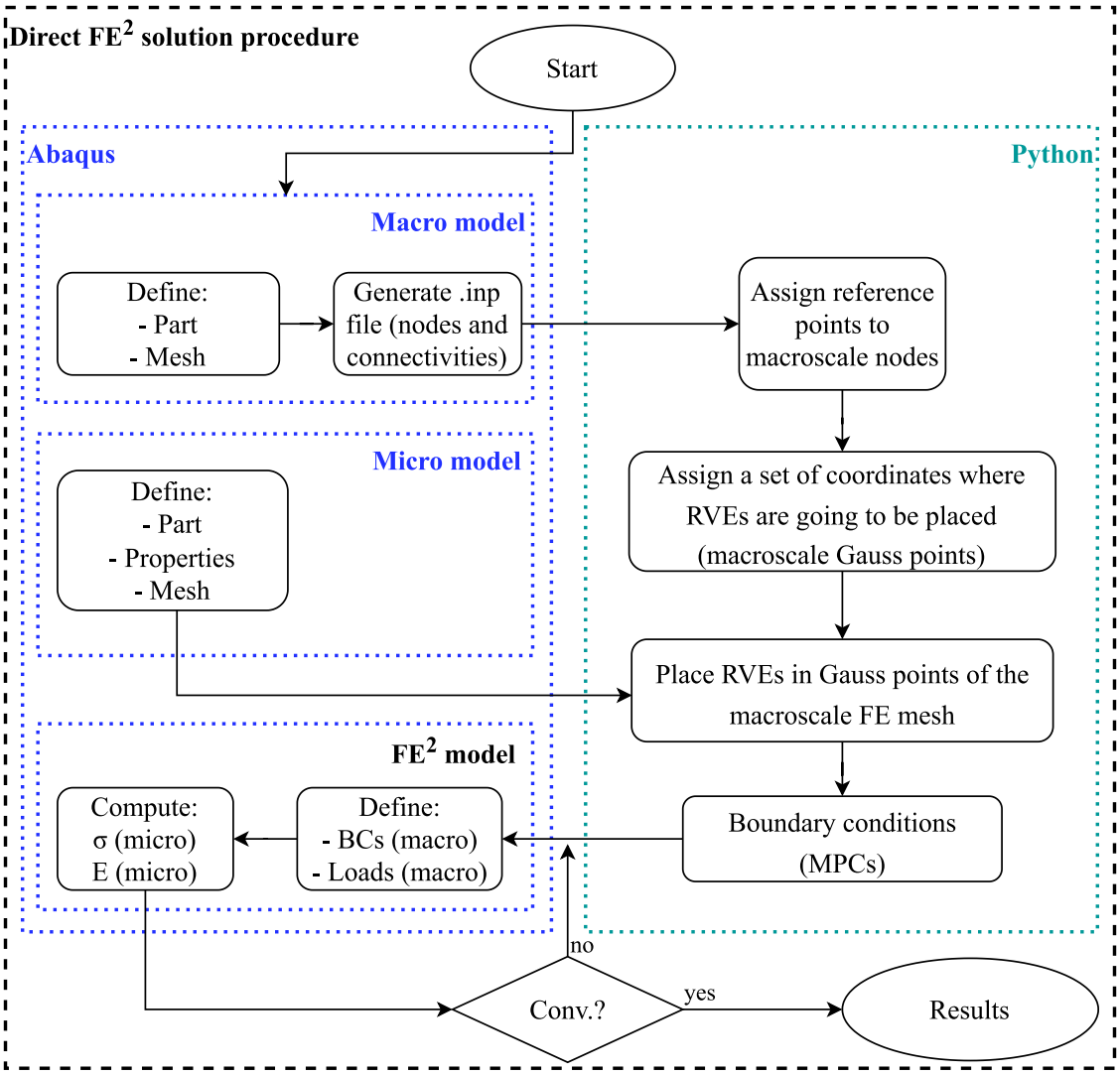

Fig. 2. Flowchart of the entire procedure.

nodes within the macroscopic elements are linearly interpolated with reduced integration, a single Gauss point is located at the natural coordinates $\xi = 0.0$ and $\eta = 0.0$. In contrast, if the same element is fully integrated, there are four Gauss points at the natural coordinates $\xi = \pm\sqrt{3}/3$ and $\eta = \pm\sqrt{3}/3$.

That information is exported as an input file. Using the information regarding the macroscale FE mesh, a Python script is developed to assign reference points (RP) to all nodal points of the macroscale. In addition, a set of coordinates is generated to place the RVEs within the direct FE^2 model. The centre of the RVE coincides with the Gauss points of the macroscale model. It is worth mentioning that the thickness of the RVE is multiplied by a scaling factor to satisfy Eq. (16).

To run the direct FE^2 model, a Python script is executed, which consists of placing one RVE at every Gauss point (GP) of the macroscale FE mesh. Fig. 3 illustrates an example of how a macroscale finite element is represented in its direct FE^2 RVE. In this instance, the macroscale element employs linear interpolation and is fully integrated, resulting in four GPs, as shown in Fig. 3(a). In the microscale model, the centres of the RVEs are positioned on the GPs of the macroscale element, as depicted schematically in Fig. 3(b). The size, geometry, and materials of the RVEs can be adjusted based on the specific problem under consideration.

Another Python script is developed to apply BCs to the micro model. This involves the application of MPCs, which interpolate the

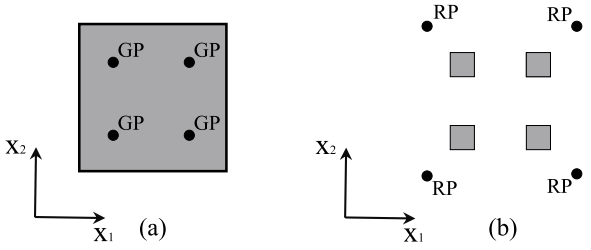

Fig. 3. (a) Representation of a single finite element at the macro scale with its associated Gauss points (GP) and (b) the direct FE^2 scheme showing the RP and the placement of RVEs on the Gauss points of a macro scale finite element.

displacement field at the nodes on the boundaries of the RVEs with the displacement field of the macro scale model (Eq. (19)). Finally, the solution procedure is carried out by considering the loads and boundary conditions at the macroscale, resulting in the fields of interest in each RVE defined in the model. After assembling the FE^2 model, the problem can be approached as a standard FE problem. Thus, if a nonlinear problem is considered, the convergence is addressed in the same way as in a typical finite element analysis.

Lastly, the direct scale transition through the application of MPCs enables a unified analysis that incorporates both micro and macro

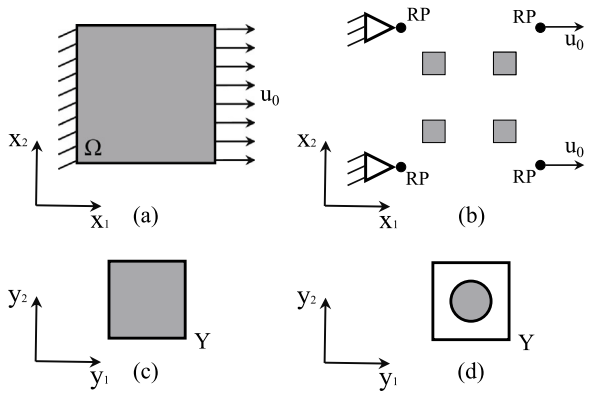

Fig. 4. Domains considered for the comparison between the methods: (a) Full domain, (b) direct FE^2 domain and RVEs for (c) homogeneous and (d) fibre-reinforced domains.

scales within a single model. This approach allows for the application of different load cases and boundary conditions directly to the macro mesh. Simultaneously, different material models can be defined and applied directly to the RVEs.

3. Results and discussion

This section is divided into three parts:

- In Section 3.1, we validate the herein implemented direct FE^2 method (see Fig. 2) against a full FE analysis, analysing both homogeneous (Section 3.1.1) and heterogeneous (Section 3.1.2) mediums.
- In Section 3.2, we focus on the heterogeneous medium and demonstrate how the direct FE^2 method can be applied to analyse specific regions within the macroscale domain, assuming known BCs.
- In Section 3.3, we analyse a virtual transverse tensile test to assess the influence of void fractions on the microscale.

In all cases, a linear elastic regime is adopted, and both the macro and micro domains are discretised by shell elements with linear interpolation. Additionally, the base materials in the analyses are considered homogeneous and isotropic.

3.1. The validation

For the validation of the implemented method, we consider a simple square plate with unitary dimensions, clamped on one side and subjected to a prescribed unitary displacement field on the other side, as shown in Fig. 4(a), which represents a portion of the coupon to be tested. For illustration purposes, we assume the macroscopic domain (Fig. 4(a)) to be discretised by a single element with linear interpolation and fully integrated. In this case, four GPs represent the entire macroscopic domain, and consequently, four RVEs are used to represent the direct FE^2 model, as depicted in Fig. 4(b). If a reduced integration scheme is adopted for the macro scale element, only one single GP is used per element, and thus only a single RVE is used to depict the part related to the direct FE^2 model. Additionally, we consider an isotropic and homogeneous RVE, as shown in Fig. 4(c), and a heterogeneous one, as shown in Fig. 4(d), representing a fibre-reinforced composite.

In all cases, linear-elastic behaviour is assumed, and the base materials are considered homogeneous. The interpolation between the macro scale nodal displacements (RP in the direct FE^2 model) and the RVE boundary nodal displacements is linear, and shell elements are used in all analyses.

Table 1
Nomenclature adopted in the analyses for the homogeneous case, macro scale discretisation and geometrical parameters for the RVEs.

Nomenclature	Macro Elements	RVE area [mm^2]	RVE thickness [mm]
RVE_1	1	0.3 × 0.3	2.776
	4	0.15 × 0.15	
	16	0.075 × 0.075	
RVE_2	1	0.1 × 0.1	25
	4	0.05 × 0.05	
	16	0.025 × 0.025	
RVE_3	1	0.05 × 0.05	100
	4	0.025 × 0.25	
	16	0.0125 × 0.0125	

3.1.1. Homogeneous medium

For the homogeneous medium, the macroscopic domain is discretised by one, four, and sixteen quadrilateral elements with full integration. The thickness of the macroscopic domain is unity, and a unitary prescribed displacement in the x_1 direction is applied to the right end of the domain. Additionally, three different RVE areas are considered in the analyses. The nomenclature adopted is shown in Table 1, alongside the macroscopic discretisation and the RVE areas and associated thicknesses. For each macroscopic element, four RVEs are used in the direct FE^2 model, and in every case, the RVEs are discretised by 10 × 10 shell finite elements (S4 element - Abaqus nomenclature). The elastic properties adopted in the analyses are E = 200 GPa and $\nu = 0.3$.

Fig. 5 shows the comparison for the displacement field (absolute) and Fig. 6 shows the comparison for the von Mises stress field for all cases in Table 1. In the displacement field, both the macro scale models and their direct FE^2 equivalents yield identical values when considering the same physical region within the domain. Similar observations apply to the stress field, although some numerical oscillations are noticeable in the direct FE^2 models. These oscillations are negligible and may be attributed to the increased computational load resulting from the greater number of elements in the direct FE^2 mesh and also due to the additional equations in the model resulting from the application of MPCs. A crucial aspect to highlight is that the scaling factor applied to the thicknesses of the RVEs ensures consistent responses for all analyses. Hence, this aspect of the method can be strategically used to show and analyse specific regions within the domain, as the RVE area can be adjusted to suit the characteristics of the macroscopic domain defined by the physical problem. Then, for this simple case, the equivalence between a full FE model and the direct FE^2 equivalents is proven to be achieved.

3.1.2. Heterogeneous medium

The same macroscopic model (Fig. 4(a)) is used to analyse a heterogeneous medium. The considered RVE is depicted in Fig. 4(d), representing a fibre-reinforced composite. Our objective is to compare the resulting fields within the same region of the domain for both a full FE analysis and its equivalent direct FE^2 model.

To facilitate a simplified comparison between the approaches, several assumptions are made:

(i) The fibres are regularly distributed within the domain (equally spaced and face-centred RVE);
(ii) One fibre is positioned in the centre of the macroscopic domain; and
(iii) Reduced integration is applied to the macroscopic elements (resulting in only one RVE per macroscopic element positioned at its centre).

As a result, two scenarios are considered for the macroscopic domain:

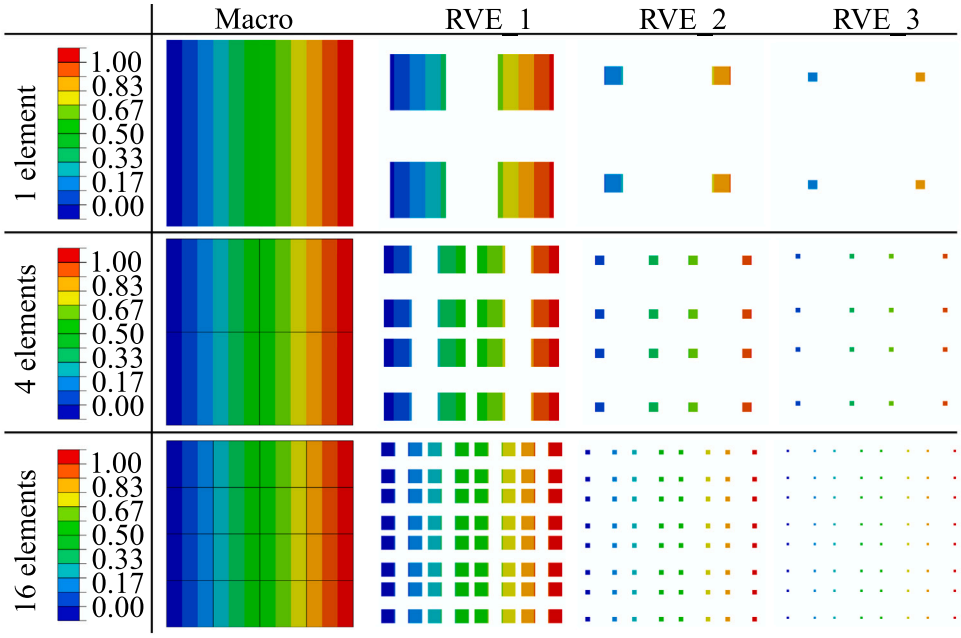

Fig. 5. Comparison of displacement fields [mm] between the macro scale models and the direct FE^2 considering different geometric parameters of the RVEs.

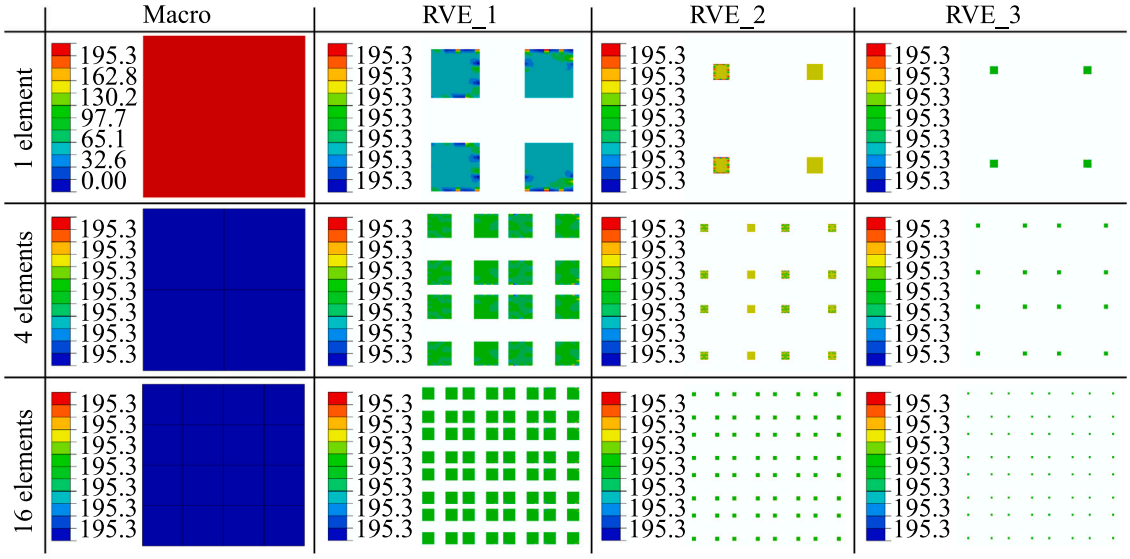

Fig. 6. Comparison of von Mises stress fields [MPa] between the macro scale models and the FE^2 considering different geometrical parameters for the RVEs.

(i) 25 fibres; and
(ii) 81 fibres.

These values were selected to ensure that the physical position and size of the fibres are the same in both the direct FE^2 and the full FE model. In every case, the direct FE^2 model is selected so that the central fibre in the full model and the direct FE^2 models coincide. Therefore, for the 25-fibre model, two direct FE^2 models are considered, containing 25 and 1 RVEs, respectively. For the 81-fibre model, three direct FE^2 models are considered, containing 81, 9, and 1 RVEs, respectively. The macroscopic models for the 25- and 81-fibre domains, and the direct FE^2 parts, are shown in Figs. 7 and 8, respectively. For each case, the analysed region is located in the central fibres of the domain, specifically R1 for the 25-fibre case and R2 for the 81-fibre case.

Table 2 summarises the used nomenclature, the number of fibres and RVEs used in the analyses, and the geometric parameters for the RVEs. The elastic properties assumed in the analyses are $E_m = 3.35$ GPa, $\nu_m = 0.35$ for the matrix and $E_f = 230$ GPa, $\nu_f = 0.2$ for the fibres. The fibre volume fraction is $V_f = 0.55$, determined experimentally through a μ-CT scan. This value represents the lower bound observed in the experiments. In both Full models and FE^2 models, the approximate element size used is 0.003 mm to ensure that equivalent regions in both models are discretised similarly.

Figs. 9 and 10 present the results for the cases presented in Table 2, showing the maximum principal stress and the maximum principal strain. For the 25-fibre model, we observe maximum relative errors when comparing the full FE model to the direct FE^2 models of 1.46% for both maximum and minimum stresses, and 4.5% for both the maximum and minimum strains. In the case of the 81-fibre model, the errors are

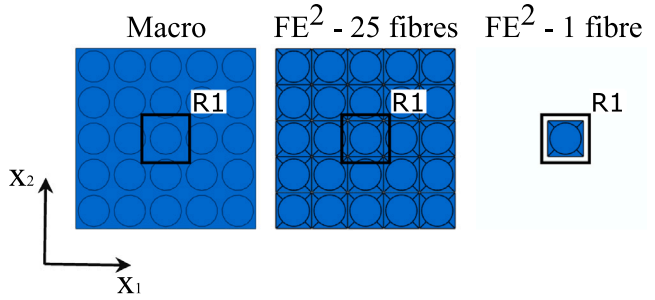

Fig. 7. Depiction of the macroscale model with 25 fibres and the FE^2 counterparts with 25 and 1 fibres, along with the region of interest in the central fibre of the domain.

Table 2
Nomenclature adopted in the analyses for the heterogeneous case, total number of fibres in the macro scale domains, number of RVEs used in the direct FE^2 analyses, and geometrical parameters for the RVEs.

Total number of fibres	FE^2 number of RVEs	RVE area [mm^2]	RVE thickness [mm]
25 fibres	25	0.20 × 0.20	1
	1		25
81 fibres	81	0.11 × 0.11	1
	9		9
	1		81

3.86% for the maximum stress, 3.85% for the minimum stress, 3.2% for the maximum strain, and 3.0% for the minimum strain.

In all scenarios, both the qualitative and quantitative results closely align when comparing both approaches, demonstrating the potential of the method. An interesting aspect of the direct FE^2 approach is that only the RVEs are discretised by finite elements. Consequently, the number of RVEs employed significantly impacts the total number of elements in the FE mesh and, hence, the processing time for the analysis. For the 25-fibre and 81-fibre models, the full FE analyses are discretised by 50,918 and 303,935 elements, respectively, whereas the direct FE^2 equivalents, with a single RVE, use only 2875 elements. The substantial difference in the number of used elements highlights the efficiency of the method, particularly when considering the relative errors in the stress and strain fields within a specific region of the domain under investigation.

3.2. The region of interest (RoI)

A virtual tensile test of a fibre-reinforced material is considered. In this case, we aim to demonstrate the applicability of the direct FE^2 method, considering different BCs to analyse specific regions of the domain. This approach allows for significant time savings in analyses. Moreover, we explore the impact of varying the RVE area on the results.

The domain considered for the virtual test is depicted in Fig. 11, where a prescribed displacement field is applied to both ends of the domain. For direct FE^2 analyses, three equivalent macroscopic domains are considered, as also illustrated in Fig. 11. In these cases, a null prescribed displacement field in the x_1 direction is applied to the left end of the domain to account for symmetry, while a prescribed displacement field at the right end of the domain is obtained by linearly interpolating the displacement field of the complete domain (u_0). Table 3 presents the geometric parameters and the prescribed displacement fields used in the macroscopic domains. For the macro scale, a reduced integration scheme is employed, resulting in one RVE per macroscopic element, placed at its centre. In all cases, a unit thickness is adopted for the macroscopic domain.

The RVE consists of a fibre-reinforced composite with a centred fibre. We consider three different RVE sizes, with areas and thicknesses adopted to satisfy Eq. (16) detailed in Table 4. The same FE mesh is

Table 3
Geometrical parameters, finite element mesh, and boundary conditions adopted for the macro scale domains.

	Area [mm^2]	Discretisation	Prescribed displacement
Domain_1	50 × 10	50 × 10	$u_1 = u_0$
Domain_2	20 × 10	20 × 10	$u_2 = 2u_0/5$
Domain_3	10 × 10	10 × 10	$u_3 = u_0/5$

Table 4
Geometrical parameters of the RVEs considered in the analyses.

	Area [mm^2]	Thickness [mm]
RVE_1	0.5 × 0.5	4
RVE_2	0.2 × 0.2	25
RVE_3	0.1 × 0.1	100

utilised across all analyses, comprising 191 shell elements with full integration (S4 element - Abaqus nomenclature) per RVE. The thickness of the RVE is relative to the thickness of the macro scale domain. The elastic properties of the matrix are $E_m = 3.35$ GPa, $\nu_m = 0.35$, and of the fibre $E_f = 230$ GPa, $\nu_f = 0.2$. The V_f of 55% remains the same as in the previous analyses.

The direct FE^2 models for each domain are presented in Fig. 12, illustrating the discretised fibres. The direct FE^2 models are discretised (from top to bottom) with 50 $\times 10, 20\times$ 10, and 10 × 10 RVEs, respectively. Furthermore, two RoIs, namely R1 and R2, representing the same physical location on all three models, are selected to analyse the response.

The maximum principal stress fields for all analysed cases in regions R1 and R2 are shown in Figs. 13 and 14. By analysing the stress fields for the three different domains while using the same RVE, both qualitative and quantitative comparisons among the three domains are highly similar. The relative error observed for the maximum stress in RoI 1 is 0.38% for RVE_1, 0.37% for RVE_2, and in RoI 2, it is 0.28% for RVE_1 and 0.26% for RVE_2. Notably, in both regions, the observed response for RVE_3 remains identical, regardless of the domain under consideration.

Since the interpolation of the displacement field on the RVE boundary is linear concerning the nodes of the macroscopic FE mesh, it is anticipated that as the area of the RVE decreases, and the displacement field converges more closely to a constant displacement field, the response within the RVEs tends to a limit. In addition, it is worth noting that the problem exhibits symmetry in the y direction, as no constraints are applied to the ends of the domain in this dimension.

For RVE_3, this interpolation does not significantly impact either the results or the symmetry of the results. However, for the other RVEs, some minor effects on the results and symmetry are observed. Nevertheless, these deviations are minimal and have a negligible impact on the overall results. In these analyses, due to the utilisation of numerous macroscopic finite elements, all displacement fields on the boundaries of the RVEs are relatively close, regardless of their size. Furthermore, the stress fields between the RVEs exhibit a high degree of similarity, demonstrating the effectiveness of applying the scaling factor to the thickness of the RVEs in this scenario.

The analyses demonstrate the feasibility of employing the method in a computationally efficient manner by replacing a portion of the domain with equivalent BCs. In the latter case, it becomes possible to designate specific regions where macroscopic elements with homogenised mechanical properties could replace areas where the micromechanical response of the medium is not of interest.

3.3. The influence of voids

We consider a virtual transverse tensile test to investigate the influence of voids on the composites on the micro scale [27–29]. The macro

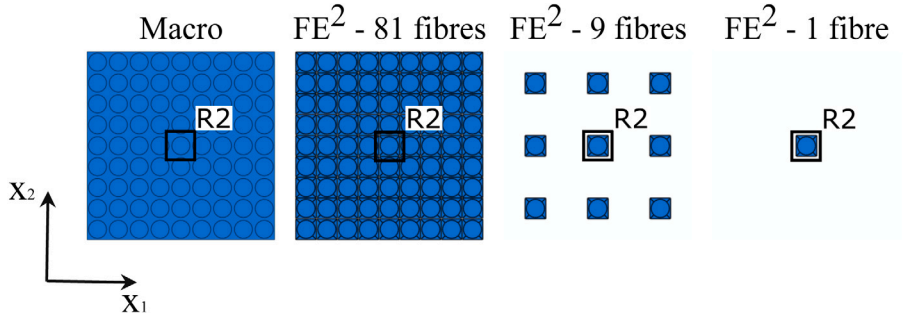

Fig. 8. Depiction of the macroscale model with 81 fibres and the FE^2 counterparts with 81, 9, and 1 fibres, along with the region of interest in the central fibre of the domain.

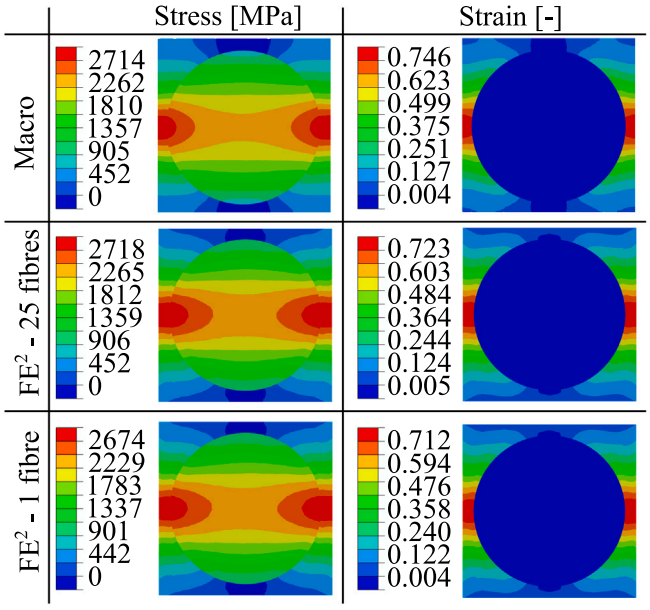

Fig. 9. Comparison of the maximum principal stress and strain fields within the central fibre of the domain, which is discretised with 25 fibres, considering a full FE model, direct FE^2 model with 25 RVEs, and FE^2 model with 1 RVE.

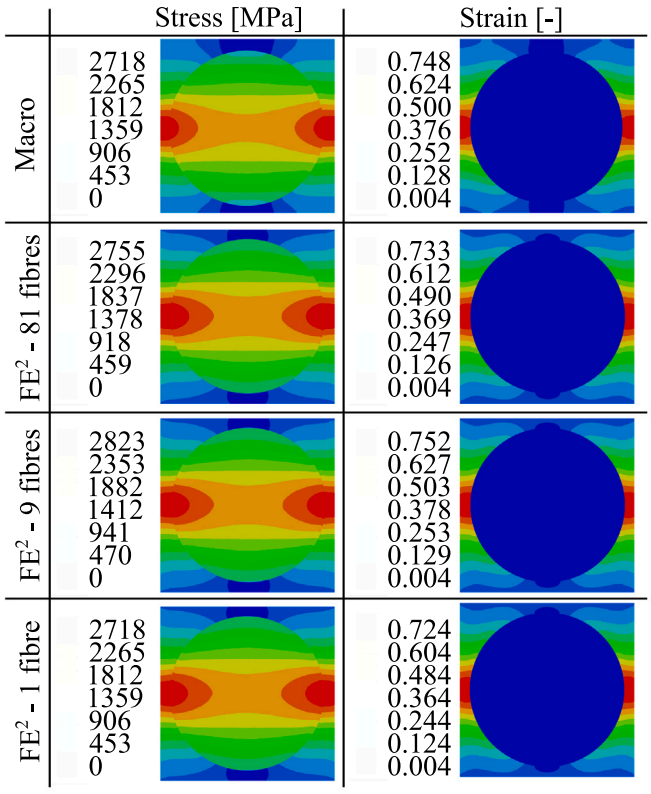

Fig. 10. Comparison of the maximum principal stress and strain fields within the central fibre of the domain, which is discretised with 81 fibres, considering a full FE model, direct FE^2 model with 81 RVEs, direct FE^2 model with 9 RVEs, and FE^2 model with 1 RVE.

scale domain has an area of $100 \times 10\,\text{mm}^2$ and is clamped on the left end, while a distributed load is applied to the right end. The macro scale domain is discretised using 20×2 macro scale finite elements. Additionally, a reduced integration scheme is adopted for the macro scale elements, resulting in one RVE associated with each macro scale element. Therefore, the direct FE^2 model consists of a total of 40 RVEs. While the response is obtained in all RVEs within the domain, we focus our analysis on two RoI: R1 and R2.

The macro scale domain with the assumed BCs, the macro scale FE mesh, and the equivalent direct FE^2 model, depicting the two RoIs for the analyses, are shown in Fig. 15. To investigate how voids at the microscale impact stress distribution, we are considering six distinct void distributions within the RVEs. In the first and second RVEs, ellipse-shaped voids are placed in the most and least stressed areas of intact RVEs analysed in Section 3.2. In the remaining RVEs, random distributions of four circular voids are considered. Fig. 16 depicts the six RVEs containing the void pattern distributions.

Within each RVE, we examine four different volume fractions (experimentally determined using μ-CT scans, with the upper bound set at approximately the maximum value observed experimentally [30]): $v_v = 1\%$, 2%, 3%, and 4%. In all scenarios, the damage pattern remains consistent, meaning its position remains unchanged, and only the v_v varies. Consequently, the centres of both ellipses and circles remain in their original positions. The area of the RVEs in all analyses is $1 \times 1\,\text{mm}^2$, which results in a relative thickness of the RVEs concerning the macro scale thickness of 25 to satisfy Eq. (16). The approximate global element size used for the finite element discretisation of the RVEs is 0.02 mm, resulting in an FE mesh of approximately 3000 elements per RVE in the direct FE^2 model. The objective is to maintain a consistent size for each finite element used in the discretisation to minimise stress concentration effects between different analyses and ensure an accurate interpretation of the results.

The elastic properties considered for the fibres are $E_f = 230\,\text{GPa}$ and $\nu_f = 0.2$, whereas for the epoxy matrix are $E_m = 2.57\,\text{GPa}$ and $\nu_m = 0.35$. To represent voids, we use finite elements with elastic properties significantly smaller in magnitude compared to the other components in such a way that they do not contribute to the mechanical behaviour of the component.

In addition, we consider a failure criterion for the matrix. As demonstrated in [31], the epoxy matrix follows a linear elastic behaviour until it reaches a specific maximum stress threshold, beyond which

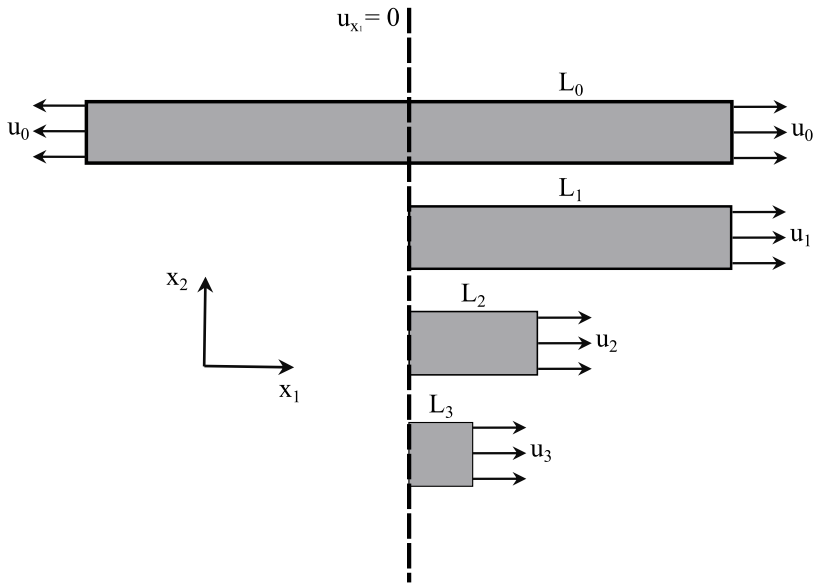

Fig. 11. Virtual tensile test of a fibre-reinforced composite with several boundary conditions and geometric parameters to analyse specific regions of interest within the domain.

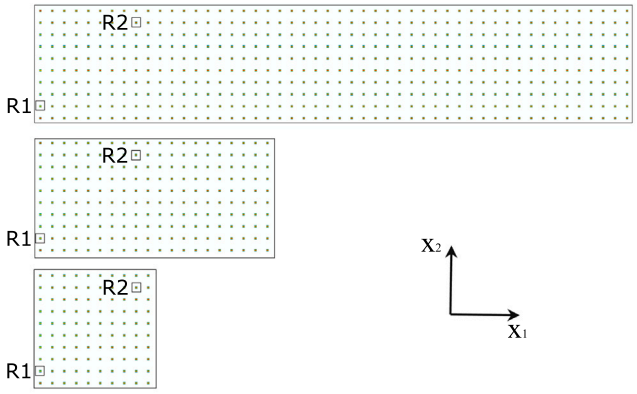

Fig. 12. Direct FE^2 model depicting the fibre distribution and the regions analysed in each case.

it undergoes a sudden brittle failure. Consequently, we designate the maximum admissible stress for the matrix as $\sigma_{adm} = 41.4$ MPa, and the maximum stress failure criterion is used in the analyses. The micro scale stress is computed based on the apparent stress applied in the macroscopic domain, which we define here as the total force applied to the macro scale divided by its cross-section.

Figs. 17, 18 show the distribution of the maximum principal stress for all considered RVEs in the regions of interest R1 and R2, respectively, under apparent stress of 10 MPa. When comparing the different RVEs, it becomes evident that the voids inserted in RVE_1 have the most significant impact on the maximum stress observed in the RoIs. In this case, a maximum stress of 54 MPa is observed in R1, for a v_v of 4%, which is approximately five times greater than the applied apparent stress. This behaviour is somewhat expected since the voids were strategically located in the most stressed areas of the domain, which are where the highest stresses are observed in the intact RVE. Similarly, the lowest influence of voids on the maximum stresses is observed in the RVE_2, with the highest value of 19 MPa in R2 for the case with a v_v of 4%. In this case, the behaviour is the opposite of what was observed in RVE_1, as the voids are placed in the less stressed regions of an intact RVE.

The remaining analysed RVEs show intermediate responses regarding the impact of voids on the maximum stress. In RVE_3 and RVE_4, for example, some voids make contact with either fibres or boundaries of the RVE. In contrast, in RVE_5 and RVE_6, all voids are fully embedded into the matrix area. Hence, more severe stress concentrations are observed for RVE_3 and RVE_4 when comparing them to RVE_5 and RVE_6, thus leading to higher maximum stresses in the analysed regions.

The maximum stresses for RVE_3 and RVE_4 exhibit a notable similarity, where the highest observed stress reaches 31.0 MPa for RVE_3 in R2 for a v_v of 4%. Likewise, a similar pattern emerges between RVE_5 and RVE_6, with the maximum stress being of 21.5 MPa for RVE_5 in R1 for a v_v of 4%.

When we compare the same RVEs with different void volume fractions, we can see that RVE_1 is the most significantly influenced. There is a substantial difference of 32.9% (in R2) in the maximum principal stress when we compare RVEs with void volume fractions of 1% and 4%. In contrast, RVE_2 is the least affected, with a minimal difference of only 2.42% (in R1) in the maximum principal stress between RVEs with void fractions of 1% and 4%. For all the other cases, the differences between RVEs with 1% and 4% of voids range from 8.2% to 12.1%, respectively.

Fig. 19 provides a summarised overview of the results obtained in these analyses. The variations in the maximum principal stress across the entire direct FE^2 model are presented, representing the highest stress observed within every RVE used in the discretisation of the macroscopic FE model. Fig. 19 illustrates how this maximum stress changes in response to the apparent stress applied to the macroscopic domain. Furthermore, the maximum admissible stress adopted for the material is also shown, enabling us to determine the threshold of apparent stress applied to the macro domain that leads to the initial failure in the matrix.

4. Conclusion

In this study, we implemented a concurrent multiscale modelling method known as the direct FE^2 approach to analyse the micromechanical behaviour of a heterogeneous medium. The problem considers domains at the macro and micro scales. By equating the virtual internal and external works, the equilibrium relationship can be derived based on the contributions of the stiffnesses from all RVEs within the domain. To ensure energy balance, a scaling factor is introduced. Furthermore, the RVEs are positioned at the Gauss points of the macroscopic FE mesh, with linear BCs applied to the nodes along the RVE boundaries.

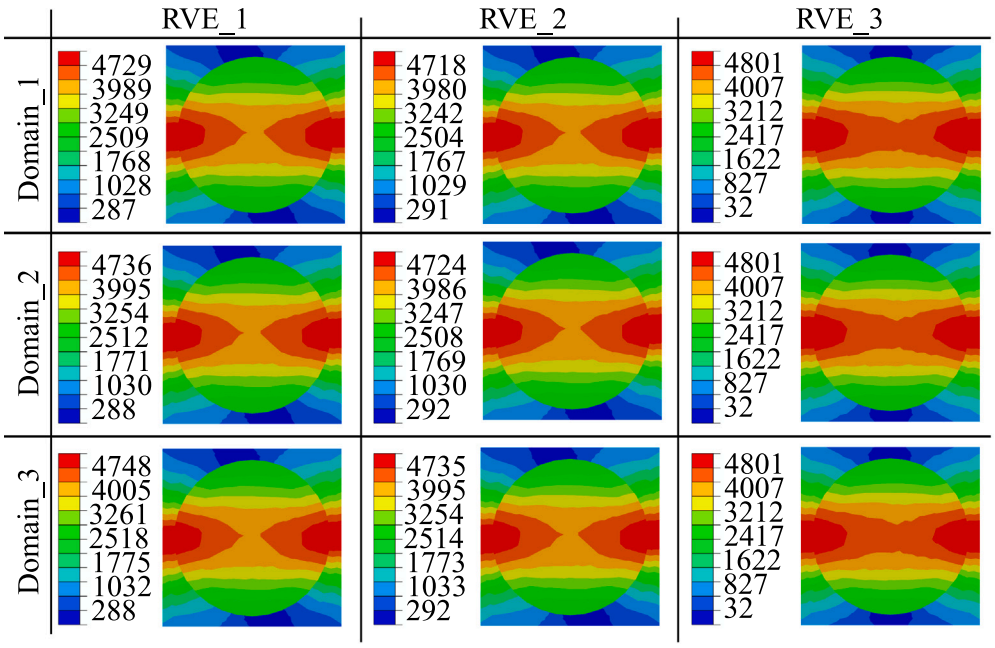

Fig. 13. Comparison of the maximum principal stress field in RoI 1 (R1) across the three considered domains using three different RVEs. All results in MPa.

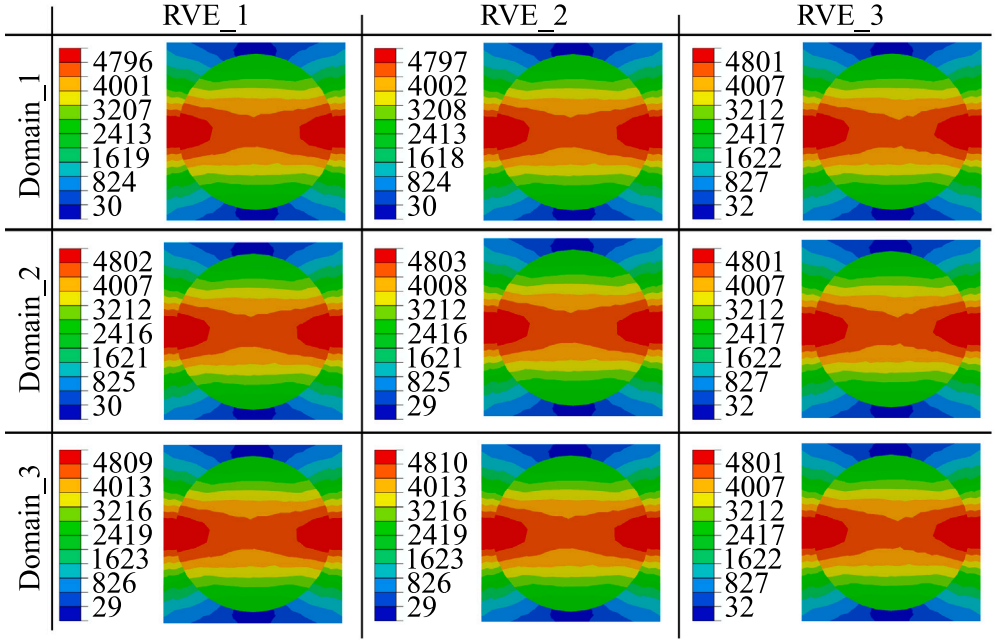

Fig. 14. Comparison of the maximum principal stress field in RoI 2 (R2) across the three considered domains using three different RVEs. All results in MPa.

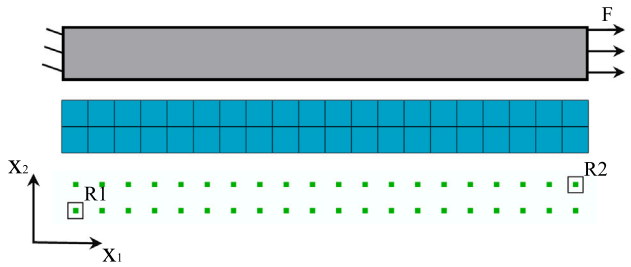

Fig. 15. Representation of the macroscopic domain with the boundary conditions, macroscopic FE mesh, and direct FE^2 model showing the RoIs R1 and R2.

These BCs are linked to the macro scale nodes through MPCs. This approach allows us to solve only one equilibrium problem, with BCs and loads applied only at the macro scale.

The validation was performed by comparing the results obtained using the direct FE^2 method with those obtained from a conventional FE analysis, where all domain heterogeneities are discretised and included in the calculations. For the initial validation, we analysed a simple plate made of homogeneous material, varying the geometric parameters of the RVEs and using different macroscopic FE meshes. The analyses revealed that both methods yield identical stress and displacement fields, confirming their equivalence. For the second validation, we considered a plate with a regular distribution of fibres. In this case, two macroscopic domains were considered, with the first containing

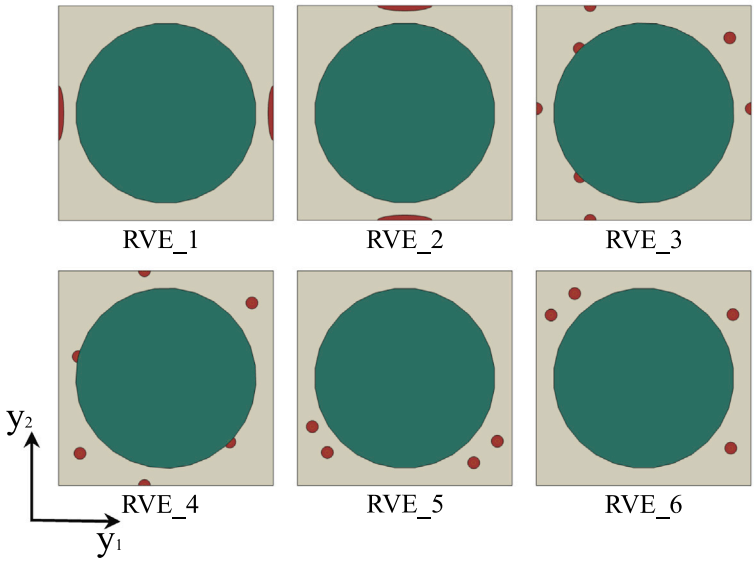

Fig. 16. Fibre-centred RVEs with various void patterns within the matrix, highlighted in dark red. In the first two RVEs, ellipse-shaped voids are located in the regions where the maximum and minimum stresses were observed in the intact model, respectively. For the remaining RVEs, four circular-shaped voids are randomly positioned within the matrix.

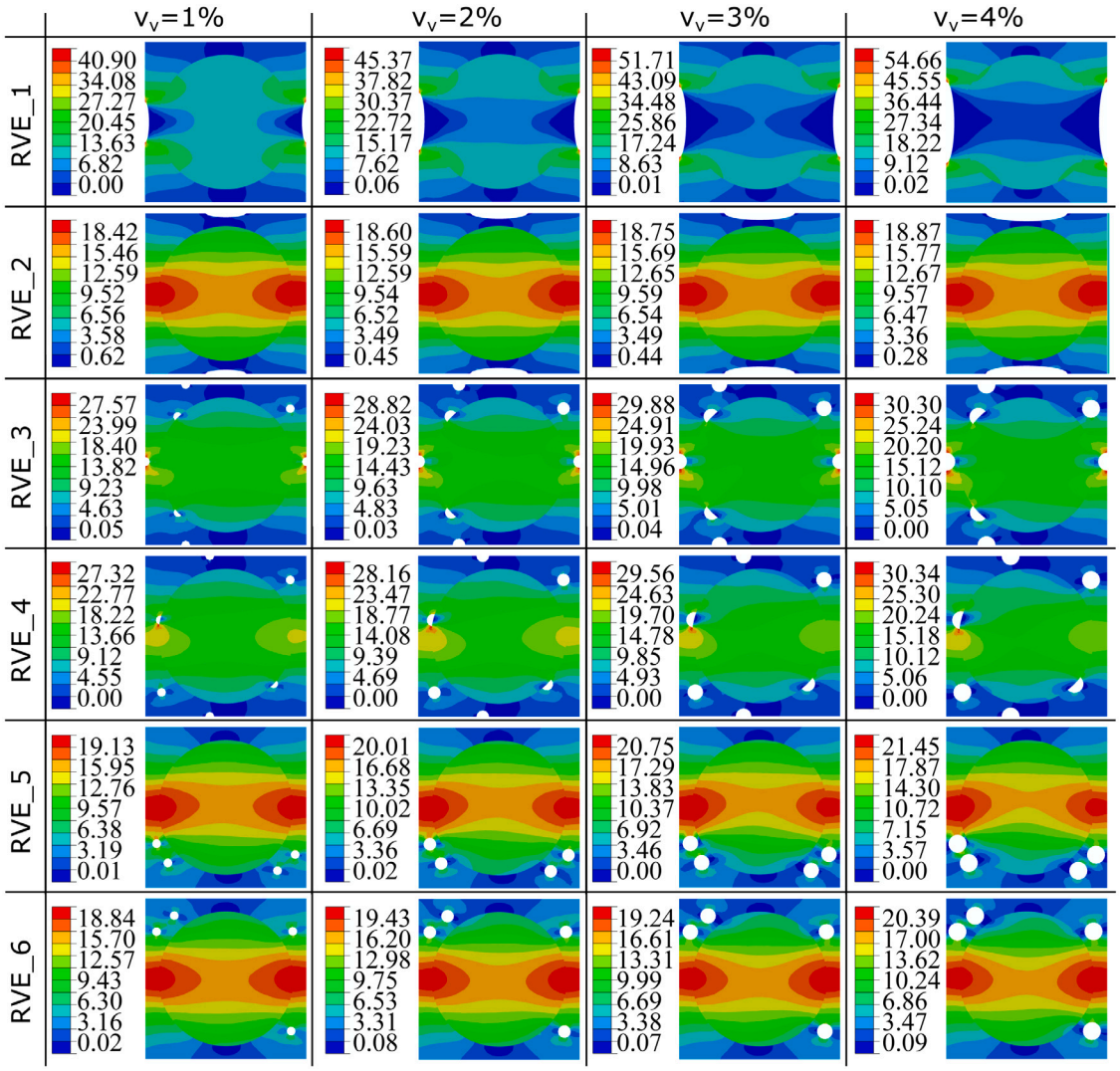

Fig. 17. Maximum principal stress distribution on the R1 region of the macroscopic domain, considering the 6 different damage profiles in the RVEs and 4 different volume fractions of voids. All values in MPa.

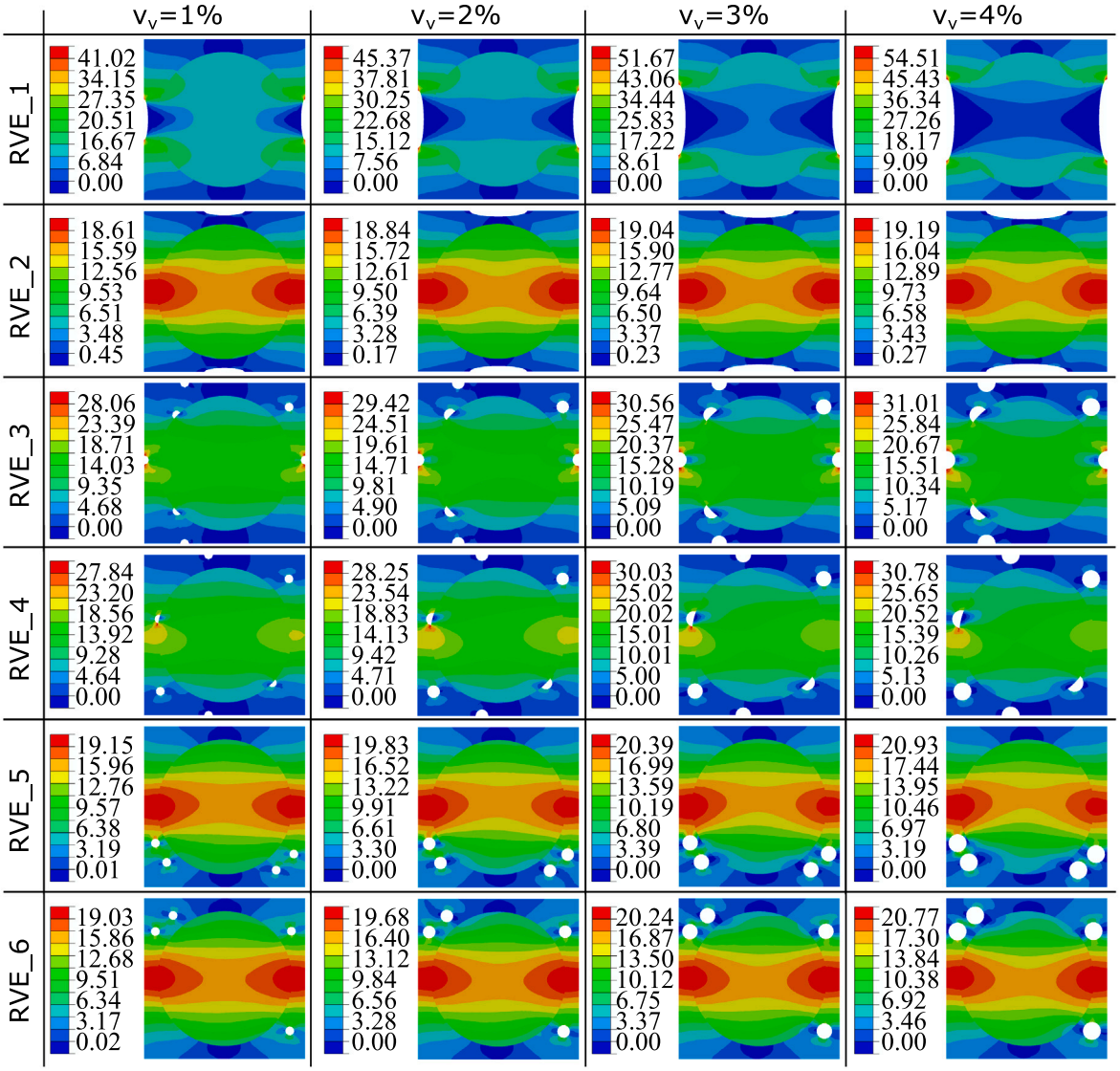

Fig. 18. Maximum principal stress distribution on the R2 region of the macroscopic domain, considering the 6 different profiles in the RVEs for the four different void volume fractions. All values in MPa.

25 fibres and the second with 81. Several models for the direct FE^2 approach were considered and compared with the full FE models. The relative error between the maximum stresses obtained was 1.46% for the case with 25 fibres and 3.86% with 81 fibres. Moreover, the computational cost was significantly lower than the full FE model.

Through a virtual transverse tensile test on a fibre-reinforced composite at several RoIs, we concluded that the direct FE^2 method proved to be a powerful analysis tool because the microscale response can be obtained directly as a function of the macro scale in a single-step. Furthermore, a parametric study has been conducted to evaluate the effect of voids within the matrix on the stress distribution in the microscale. Six different void patterns were investigated, each with four different volume fractions and distribution of voids. Through these analyses, we illustrated how the stress within the microstructure changes concerning the applied apparent stress at the macro scale.

Finally, we concluded the direct FE^2 method is a promising tool in the structural multiscale analysis of heterogeneous media. A key advantage is the significantly reduced computational cost compared to conventional FE analyses that explicitly account for all domain heterogeneities. However, it remains computationally costly compared to sequential multiscale methods. Considering that the developed method is integrated into Abaqus FE package, it allows for the utilisation of all available tools, such as different materials and finite elements. In this work, the methodology was formulated and implemented to facilitate its application in nonlinear problems. It also allows for the utilisation of failure and damage models directly at the microscopic level, thus eliminating the need for any scale transitioning in the process.

CRediT authorship contribution statement

Bruno G. Christoff: Conceptualization, Methodology, Formal analysis, Investigation, Software, Data curation, Writing – original draft, Visualization. **José Humberto S. Almeida Jr.:** Formal analysis, Investigation, Data curation, Methodology, Writing – original draft, Validation. **Marcelo L. Ribeiro:** Software. **Maísa M. Maciel:** Investigation. **Rui M. Guedes:** Supervision, Writing – review & editing. **Volnei Tita:** Resources, Supervision, Project administration, Funding acquisition, Writing – review & editing.

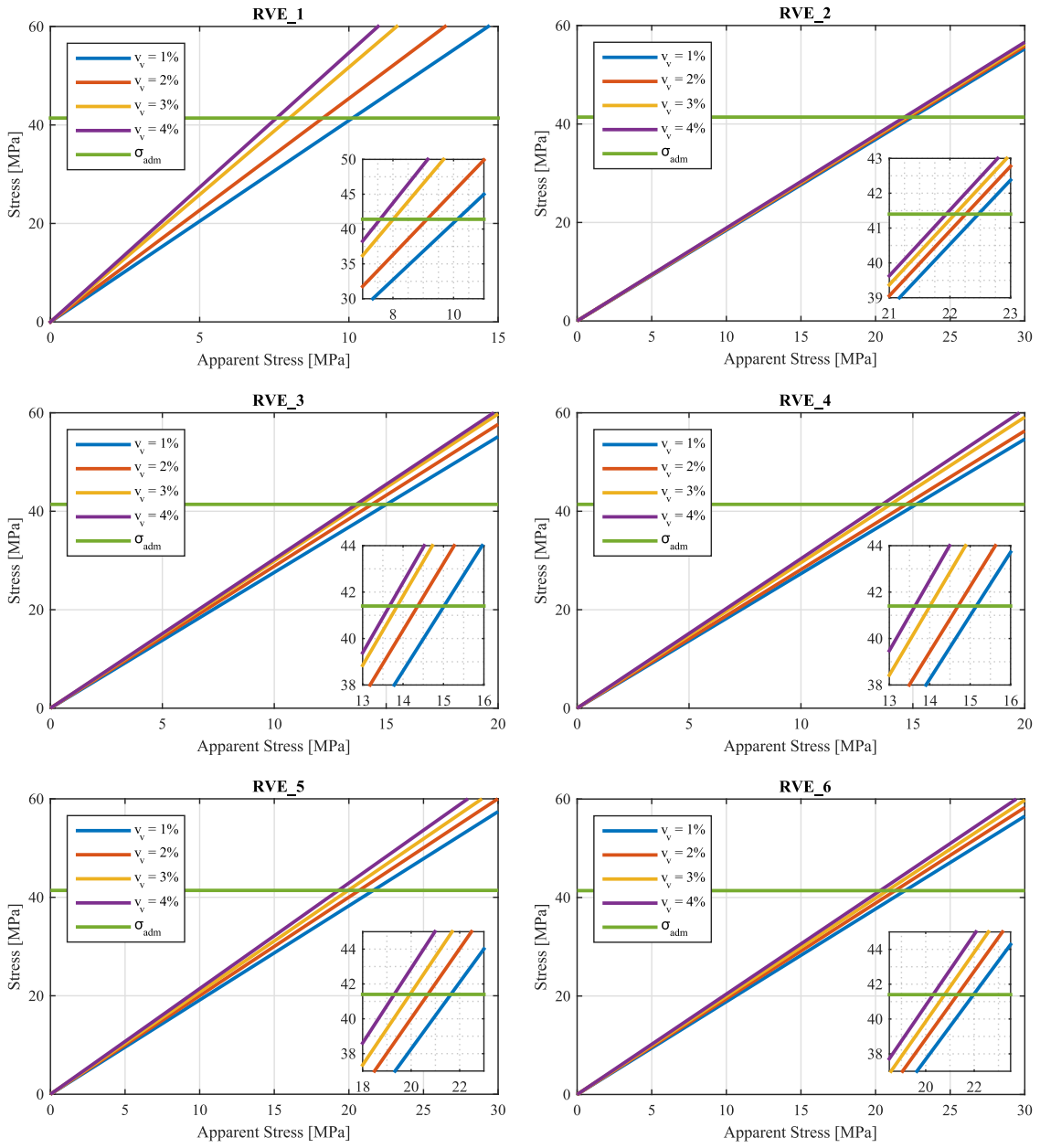

Fig. 19. Maximum principal stress observed in every RVEs in the FE^2 domain as a function of the apparent stress applied to the macroscopic domain for different volume void fractions compared to the allowable stress for the matrix. The highlighted areas represent the regions where the first finite element of the mesh reaches the maximum admissible stress.

Declaration of competing interest

The authors declare that they have no known competing financial interests or personal relationships that could have appeared to influence the work reported in this paper.

Data availability

Data will be made available on request.

Acknowledgments

VT acknowledges CNPq, Brazil (process number: 310159/2022-9 and 407531/2022-0) and CAPES/FCT (AUXPE 88881.467834/2019-01). BGC thanks CAPES and FCT agencies (AUXPE 88881.467834/2019-01) – Finance Code 001. HA is grateful to the Royal Academy of Engineering, United Kingdom (Grant No. RF/201920/19/150). MLR acknowledges FAPESP, Brazil (process number 2023/08545-8).

References

[1] B.G. Christoff, H. Brito-Santana, V. Tita, Analysis of unbalanced laminate composites with imperfect interphase: Effective properties via asymptotic homogenization method, Proc. Inst. Mech. Eng. L 236 (7) (2022) 1390–1399, http://dx.doi.org/10.1177/1464420721106000.

[2] S. Saeb, P. Steinmann, A. Javili, Aspects of computational homogenization at finite deformations: A unifying review from Reuss' to Voigt's bound, Appl. Mech. Rev. 68 (5) (2016) 050801, http://dx.doi.org/10.1115/1.4034024.

[3] M. Silani, S. Ziaei-Rad, H. Talebi, T. Rabczuk, A semi-concurrent multiscale approach for modeling damage in nanocomposites, Theor. Appl. Fract. Mech. 74 (2014) 30–38, http://dx.doi.org/10.1016/j.tafmec.2014.06.009.

[4] B.G. Christoff, H. Brito-Santana, R. Talreja, V. Tita, Multiscale embedded models to determine effective mechanical properties of composite materials: Asymptotic homogenization method combined to finite element method, Composites Part C 9 (2022) 100303, http://dx.doi.org/10.1016/j.jcomc.2022.100303.

[5] R. Patil, B. Mishra, I. Singh, A multiscale framework based on phase field method and XFEM to simulate fracture in highly heterogeneous materials, Theor. Appl. Fract. Mech. 100 (2019) 390–415, http://dx.doi.org/10.1016/j.tafmec.2019.02.002.

[6] B.G. Christoff, J.H.S. Almeida Jr., E.L. Cardoso, V. Tita, A multiscale topology optimisation framework for hollow spheres as cellular materials, Eng. Struct. 284 (2023) 115990, http://dx.doi.org/10.1016/j.engstruct.2023.115990.

[7] A. Stamopoulos, K. Tserpes, S. Pantelakis, Multiscale finite element prediction of shear and flexural properties of porous CFRP laminates utilizing X-ray CT data, Theor. Appl. Fract. Mech. 97 (2018) 303–313, http://dx.doi.org/10.1016/j.tafmec.2017.04.020.

[8] R. Xu, Y. Hui, H. Hu, Q. Huang, H. Zahrouni, T. Ben Zineb, M. Potier-Ferry, A Fourier-related FE^2 multiscale model for instability phenomena of long fiber reinforced materials, Compos. Struct. 211 (2019) 530–539, http://dx.doi.org/10.1016/j.compstruct.2018.12.028.

[9] F. Feyel, A multilevel finite element method (FE^2) to describe the response of highly non-linear structures using generalized continua, Comput. Methods Appl. Mech. Engrg. 192 (28) (2003) 3233–3244, http://dx.doi.org/10.1016/S0045-7825(03)00348-7, Multiscale Computational Mechanics for Materials and Structures.

[10] F. Feyel, J.-L. Chaboche, FE^2 multiscale approach for modelling the elastovisco-plastic behaviour of long fibre SiC/Ti composite materials, Comput. Methods Appl. Mech. Engrg. 183 (3) (2000) 309–330, http://dx.doi.org/10.1016/S0045-7825(99)00224-8.

[11] S. Nezamabadi, M. Potier-Ferry, H. Zahrouni, J. Yvonnet, Compressive failure of composites: A computational homogenization approach, Compos. Struct. 127 (2015) 60–68, http://dx.doi.org/10.1016/j.compstruct.2015.02.042.

[12] J. Storm, M. Ranjbarian, V. Mechtcherine, C. Scheffler, M. Kaliske, Modelling of fibre-reinforced composites via fibre super-elements, Theor. Appl. Fract. Mech. 103 (2019) 102294, http://dx.doi.org/10.1016/j.tafmec.2019.102294.

[13] K. Raju, T. Tay, V. Tan, A review of the FE^2 method for composites, Multiscale Multidiscip. Model. Exp. Des. 4 (2021) 1–24, http://dx.doi.org/10.1007/s41939-020-00087-x.

[14] F. Feyel, Multiscale FE^2 elastoviscoplastic analysis of composite structures, Comput. Mater. Sci. 16 (1) (1999) 344–354, http://dx.doi.org/10.1016/S0927-0256(99)00077-4.

[15] S. Nezamabadi, J. Yvonnet, H. Zahrouni, M. Potier-Ferry, A multilevel computational strategy for handling microscopic and macroscopic instabilities, Comput. Methods Appl. Mech. Engrg. 198 (27) (2009) 2099–2110, http://dx.doi.org/10.1016/j.cma.2009.02.026.

[16] V.B.C. Tan, K. Raju, H.P. Lee, Direct FE^2 for concurrent multilevel modelling of heterogeneous structures, Comput. Methods Appl. Mech. Engrg. 360 (2020) 112694, http://dx.doi.org/10.1016/j.cma.2019.112694.

[17] E. Tikarrouchine, G. Chatzigeorgiou, F. Praud, B. Piotrowski, Y. Chemisky, F. Meraghni, Three-dimensional FE^2 method for the simulation of non-linear, rate-dependent response of composite structures, Compos. Struct. 193 (2018) 165–179, http://dx.doi.org/10.1016/j.compstruct.2018.03.072.

[18] T. Herwig, W. Wagner, On a robust FE^2 model for delamination analysis in composite structures, Compos. Struct. 201 (2018) 597–607, http://dx.doi.org/10.1016/j.compstruct.2018.06.033.

[19] J. Zhi, K. Raju, T. Tay, Transient multi-scale analysis with micro-inertia effects using direct FE^2 method, Comput. Mech. 67 (2021) 1645–1660, http://dx.doi.org/10.1007/s00466-021-02012-6.

[20] J. Zhi, L.H. Poh, T.-E. Tay, V.B.C. Tan, Direct FE^2 modeling of heterogeneous materials with a micromorphic computational homogenization framework, Comput. Methods Appl. Mech. Engrg. 393 (2022) 114837, http://dx.doi.org/10.1016/j.cma.2022.114837.

[21] J. Zhi, B. Yang, Y. Li, T.-E. Tay, V.B.C. Tan, Multiscale thermo-mechanical analysis of cure-induced deformation in composite laminates using direct FE^2, Composites A 173 (2023) 107704, http://dx.doi.org/10.1016/j.compositesa.2023.107704.

[22] J. Koyanagi, K. Kawamoto, R. Higuchi, V.B.C. Tan, T.-E. Tay, Direct FE^2 for simulating strain-rate dependent compressive failure of cylindrical CFRP, Composites Part C 5 (2021) 100165, http://dx.doi.org/10.1016/j.jcomc.2021.100165.

[23] K. Raju, J. Zhi, Z. Su, T. Tay, V. Tan, Analysis of nonlinear shear and damage behaviour of angle-ply laminates with direct FE^2, Compos. Sci. Technol. 216 (2021) 109050, http://dx.doi.org/10.1016/j.compscitech.2021.109050.

[24] B.G. Christoff, H. Brito-Santana, R. Talreja, V. Tita, Development of an Abaqus™ plug-in to evaluate the fourth-order elasticity tensor of a periodic material via homogenization by the asymptotic expansion method, Finite Elem. Anal. Des. 181 (2020) 103482, http://dx.doi.org/10.1016/j.finel.2020.103482.

[25] H. Brito-Santana, B.G. Christoff, A.J. Mendes Ferreira, F. Lebon, R. Rodríguez-Ramos, V. Tita, Delamination influence on elastic properties of laminated composites, Acta Mech. 230 (2019) 821–837, http://dx.doi.org/10.1007/s00707-018-2319-8.

[26] J.H.S. Almeida Jr., B.G. Christoff, V. Tita, L. St-Pierre, A concurrent fibre orientation and topology optimisation framework for 3D-printed fibre-reinforced composites, Compos. Sci. Technol. 232 (2023) 109872, http://dx.doi.org/10.1016/j.compscitech.2022.109872.

[27] F.M. Monticeli, J.H.S. Almeida Jr, R.M. Neves, F.G. Ornaghi, H.L. Ornaghi, On the 3D void formation of hybrid carbon/glass fiber composite laminates: A statistical approach, Composites A 137 (2020) 106036, http://dx.doi.org/10.1016/j.compositesa.2020.106036.

[28] F.M. Monticeli, R.M. Neves, H.L. Ornaghi Jr, J.H.S. Almeida Jr, A systematic review on high-performance fiber-reinforced 3D printed thermoset composites, Polym. Compos. 42 (8) (2021) 3702–3715, http://dx.doi.org/10.1002/pc.26133.

[29] J.H.S. Almeida Jr, S. Jayaprakash, K. Kolari, J. Kuva, K. Kukko, J. Partanen, The role of printing parameters on the short beam strength of 3D-printed continuous carbon fibre reinforced epoxy-PETG composites, Compos. Struct. 337 (2024) 118034, http://dx.doi.org/10.1016/j.compstruct.2024.118034.

[30] M.M.Á.D. Maciel, S. Amico, R.M. Guedes, V. Tita, Evolution of variable angle tow composite structures: Data analysis and relevance of the theme, Proc. Inst. Mech. Eng. L (2024) 14644207241240048, http://dx.doi.org/10.1177/14644207241240048, in press.

[31] S. Gurusideswar, N. Srinivasan, R. Velmurugan, N. Gupta, Tensile response of epoxy and glass/epoxy composites at low and medium strain rate regimes, Procedia Eng. 173 (2017) 686–693, http://dx.doi.org/10.1016/j.proeng.2016.12.148.